J. Chemtracks 27 (1&2) 9-18, 2025

Abstracted / Indexed in
A division of the American Chemical Society
Chemical Abstract U.S.A.

ISSN 0973-239X
CODEN:JCOHF7
IMPACT FACTOR : 7.866

Facile Synthesis of Mn_2O_3 as an Electrode Material for Supercapacitor Application

Benjamin Raj[1], Rekha Kumari[2] and Guru Charan Sahu[2]*

[1]Department of Chemistry, Radha Govind University, Ramgarh-829122, Jharkhand, India

[2]University Department of Chemistry, Ranchi University, Ranchi-834008, Jharkhand, India

E-mail : gcs196606@gmail.com

Manuscript received online 22 December 2024, accepted on 12 January 2025

Abstract: Manganese (III) oxide (Mn_2O_3), a transition metal oxide, is well-known for its characteristics properties and potential application in various fields including catalysis, energy storage and sensing. Herein we report a cost-effective sol-gel method for the synthesis of Mn_2O_3 nanoparticles using manganese nitrate ($Mn(NO_3)_2.4H_2O$) in 100 ml of ethylene glycol for the supercapacitor application. The as-synthesized materials were confirmed by various physicochemical techniques like FTIR, XRD and BET surface area. Morphological research using SEM showed higher surface area and porousness with a uniform distribution of particles. The prepared electrode materials were deposited on a nickel foam substrate to investigate the electrochemical properties in 1 M KOH electrolyte. The galvanostatic charge/discharge (GCD), cyclic voltammetry (CV), and complex impedance studies confirmed excellent specific capacitance and capacitive behavior of the prepared material. The synthesized Mn_2O_3 exhibited an excellent specific capacitance of 75.28 F/g and 35.28 F/g at a scan rate of 5 mV/s with two different temperatures 500 and 700^{0}C. The high porosity of the materials provided a better electrolyte-electrode interface with a larger specific area, thus suggesting its suitability for energy storage applications.

(Keywords : Sol-gel, Manganese nitrate, Mn_2O_3, Nanoparticles, supercapacitor)

Introduction

The demand for energy around the world has risen significantly due to population growth, economic development, urbanization, technological advancements, changing lifestyles, and globalization[1], [2]. The most recent survey carried out by the International Energy Agency (IEA) indicates that there is a growing recognition of the necessity for a new energy security paradigm in order to address the problems associated with energy reliability, affordability, and emissions reduction. As a result of the rise of the current technological revolution and the excessive consumption of natural resources, particularly fossil fuels, the development of new energy storage technologies has become a serious problem[3–6]. The growing disparity between energy production and consumption necessitates robust energy storage solutions, especially for bridging gaps in supply that can extend from days to months, demanding technologies beyond conventional batteries with their inherent limitations such as low power density, extended charging times, potential thermal issues, and environmental impact.

There has been a significant amount of interest in supercapacitors due to the fact that they possess highly desirable characteristics such as quick charge and discharge, extended cycle life, and high-power density. The use of supercapacitors, which are a type of current energy storage system, has been significant in a variety of application fields, including hybrid electric vehicles, portable electronic gadgets, and other micro-energy storage systems[3,7,8]. Pseudocapacitor mechanisms and electric double-layer capacitors are two examples of the two distinct methods that supercapacitors can store charges. The capacitance of electric double-layer capacitors is produced by the adsorption of ions at the interface between the electrode and the

electrolyte, whereas the capacitance of pseudocapacitors is produced by redox processes that take place between the electrode and the electrolyte[9,10]. Carbon-based substances, such as activated carbon, carbon aerogel, carbon nanotubes, and graphene oxide, are responsible for the generation of electric double-layer capacitors, whereas metal oxides and conducting polymers are responsible for the generation of pseudocapacitance. Till now, numerous kinds of materials have been utilized extensively as electrode materials for supercapacitors due to their versatility[11,12].

The transition metal oxides are the attractive electrode materials for pseudocapacitors because to their numerous features, which include low cost, abundant availability, variable oxidation states, and environmental friendliness, among other advantages. Numerous single transition metal oxides, such as NiO, CO_2O_3, TiO_2, RuO_2, MnO_2, Fe_2O_3, and others, as well as mixed transition metal oxides, such as $MnCo_2O_4$, $CuFe_2O_4$, $CoFe_2O_4$, $ZnMn_2O_4$, $NiCo_2O_4$, $ZnCo_2O_4$, and others, have been proved to be suitable for use as electrode materials for pseudocapacitors[13,14]. MnO_2 is the most promising supercapacitor electrode material due to its low expense, low toxicity, wide availability, and environmental friendliness. Various researchers have used different ways to improve MnO_2 supercapacitor specific capacitance, energy density, and cycle stability. Electrode structure, shape, and surface area greatly affect MnO_2 electrochemical performance. Different synthesis methods can manage electrode material shape, structure, and porosity to monitor supercapacitor capacitance. Toupin et al. (2004) found that energy storage requires only a thin MnO_2 electrode layer. Additionally, Lee et al. (1999) demonstrated a specific capacitance of 200 Fg^{-1} using $MnO_2 \cdot nH_2O$ as the electrode for supercapacitors in KCl electrolyte

Herein we report a facile synthetic procedure for Mn_2O_3 as an electrode material for the supercapacitor application by sol-gel process. We have synthesized Mn_2O_3 by the sol-gel process followed by the calcination with two different temperatures. The bonding and structural properties of synthesized materials were confirmed by using various physicochemical techniques like FTIR, and XRD. The surface area and porosity of the material were confirmed by the BET surface area analyser. Similarly, the surface morphology and existence of elements in the sample were analysed by SEM spectroscopic techniques.

Materials and methods

Mn_2O_3 accomplished by dissolving 25 grams of manganese nitrate ($Mn(NO_3)_2.4H_2O$) in 100 ml of ethylene glycol. This was done in order to produce Mn_2O_3 nanoparticles using the sol-gel method. Adjustments were made to the amount of the solvent in order to ensure that the manganese nitrate was thoroughly dissolved. The solution was heated further at a temperature of 80 ! while being stirred continuously until a thick gel was produced. Increasing the temperature to 100 ! caused the gel to gradually turn into a fine powder. The resulting powder was sintered in an electric furnace for a period of four hours at two distinct temperatures, 500 ! and 700 !.

Characterization

Fourier transform infrared (FT-IR, Perkin Elmer IR Spectrophotometer) spectra were obtained within the range of 500-4000 cm^{-1}. These spectra were used to determine the bonding properties of the material. For the purpose of analysis, KBr was used to press pellets with a very small quantity of samples in a ratio of 1:5. In order to determine the phase and crystallographic structure of the samples, a Bruker D8 advance X-ray powder diffractometer was utilized. The equipment utilized Cu K± radiation with a wavelength of 0.15418 nm. Brunauer-Emmett-Teller (BET) measurements were performed on mixed metal oxide using Quantachrome Nova Win at a degassing temperature of 120 !. These results were used to determine the surface area and pore

diameter of the oxide. The Horiba Jobin Yvon Raman spectrometer H4551 was utilized in order to carry out the Raman examination at a wavelength of 457.9 nuclear meters. The Zeiss EVO18 scanning electron microscope (SEM) equipped with an EDAX elemental composition analyzer was utilized in order to investigate the surface morphologies of the representative sample.

Electrochemical

The electrochemical workstation CHI 660E model was used for the electrochemical characteristics utilizing CV, CD, and EIS. A typical three-electrode system was employed for electrochemical analysis in 1M KOH aqueous solution using Pt wire as a counter electrode and Ag/AgCl as a reference electrode. As-prepared sample on Nickel foam electrode was working electrode. The working electrode was made by attaching 5 mg of material dispersed in 0.5 ml ethanol using sonication. In the potential window of -0.2 to 6 V, CV and GCD analyses were performed at 5, 10, 25, 50, 75 and 100 mV/s respectively. The applied amplitude was 0.005 V vs open circuit potential for EIS spectroscopy from 106 Hz to 1 Hz. To measure ammonia, 0.002g of sample was sonicated into 0.25ml of ethanol. After perfect dispersion, the sample was drop-cast over the Ni-foam electrode, which became the working electrode. Counter and reference electrodes were Pt wire and Ag/AgCl electrodes.

Results and Discussion

FTIR Analysis

FTIR analysis was carried out to confirm the formation of Mn_2O_3 nanomaterial (FTIR, Perkin Elmer IR Spectrophotometer) spectra were recorded within the range of 500–4000 cm^{-1} at room temperature shown in figure 10. For analysis, KBr pressed pellets with a minute amount of samples in the ratio 1:5. The Mn_2O_3 shows significant peaks at 455 cm^{-1} – 563 cm^{-1}, and 632-647 cm^{-1} that corresponds to out-of-plane bending modes, asymmetric stretching of bridge oxygen species (Mn–O–Mn), and symmetric stretching mode, respectively. The peak at around 3500 cm-1 is attributed due to the O-H stretching frequency which might be due to the presence of moisture in the atmosphere. The above-mentioned peaks confirmed the successful formation of manganese oxide (Mn_2O_3) nanoparticles.

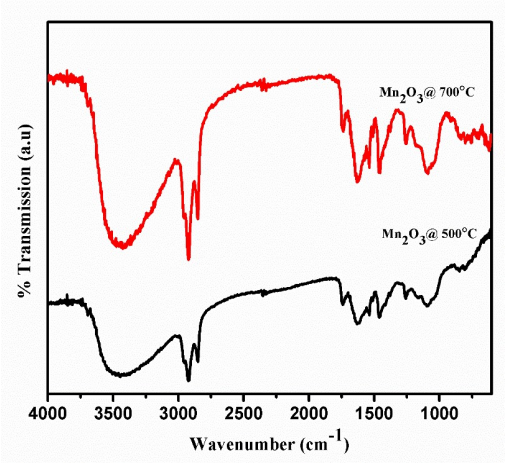

Figure.1 FTIR comparison of Mn_2O_3 at two different temperatures

XRD Analysis

The crystal structure and orientation of their nanohybrids were investigated by the XRD and presented in Figure 2. It is significant to note that the presence of an intense and sharp peak in all XRD patterns indicates that as-synthesized pure metal oxides are highly crystalline in nature. The reflection peaks for the Mn_2O_3 nanoparticles were matched with the (JCPDS card no. 96-151-4120). The peaks were also indexed with different (hkl) planes (200), (301), (220), (222), (231), (400), (323), (341), (512), (440), (424), (352), (451), (435), and (231) obtained at 2-theta values of 18.08, 29.61, 31.60, 33.06, 36.90, 38.88, 44.63, 50.81, 52.00, 54.79, 58.90, 60.89, 65.26, 71.09, and 75.06 respectively. Thus, it has been confirmed the formation of Mn_2O_3 nanoparticles. It has been

found that the intensity of peaks becomes sharper as the sample is calcined at higher temperature. The average crystalline size of the sample was calculated by using Scherrer's equation

$$D=0.9\lambda\beta/.\cos\theta \quad \ldots\ldots\ldots\ldots(1)$$

Where,

λ = wavelength of CuK_{α} radiation, β is full-width half maxima (FWHM) and theta (θ) is the angle of diffraction. The average crystalline size of Mn_2O_3 at 500 ºC and 700 ºC are 21.86 nm and 26.76 nm respectively. The particles size is also increases as the temperature has been increased which might be due to the high degree of agglomeration.

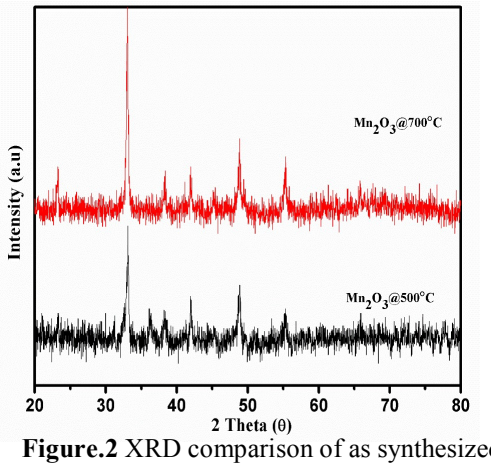

Figure.2 XRD comparison of as synthesized metal oxide at two different temperatures.

Surface Morphology Analysis

Figure. 3 shows the SEM micrographs of as synthesized Mn_2O_3 nanoparticles at two different temperatures 500 ºC and 700 ºC. Figure (3 a and b) correspond to 500 ºC and figures (3 c and d) correspond to the SEM images of Mn_2O_3 at 700 ºC respectively. SEM results show that at low temperatures the particles are seems to be smaller in size with the regular arrangement of particles. But when temperature has been increased to 700 ºC the particle size has also increased which might be due to the high degree of agglomeration and also it shows that the particles are not in the regular shape. It has been also confirmed with the XRD data as above.

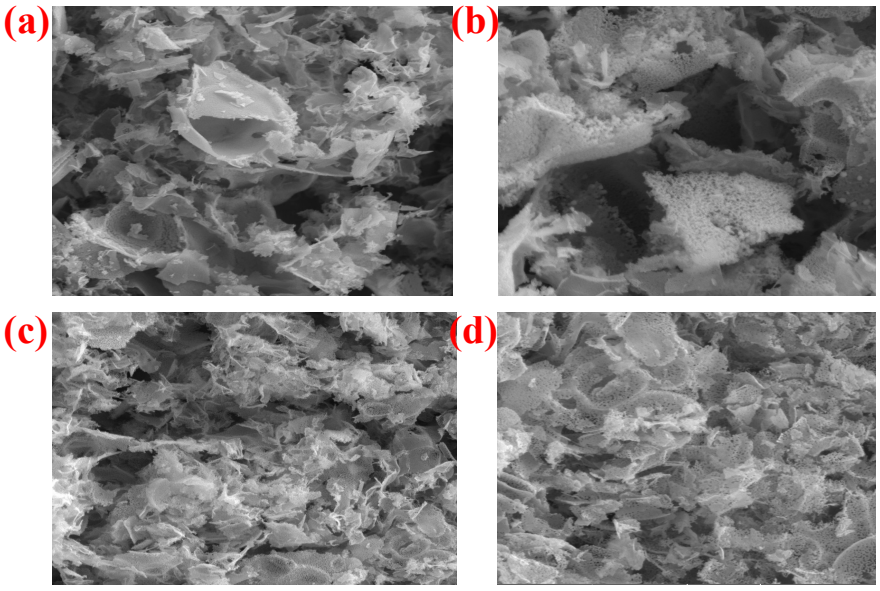

Figure. 3 SEM images of Mn_2O_3 at two different temperatures 500 ºC and 700 ºC.

Electrochemical measurement

The electrochemical properties of synthesized nanohybrids were performed by Cyclic Voltammetry (CV), Charge-Discharge (CD), impedance spectroscopy (EIS) and amperometry using an electrochemical workstation CHI 660E model. A conventional three-electrode system was used to perform the electrochemical analysis in 1M KOH aqueous solution as an electrolyte where Pt wire was used as a counter electrode, Ag/AgCl as a reference electrode. The as-prepared sample mounted on the graphite electrode was used as the working electrode. The working electrode was prepared by adhering a small amount of sample (from 5 mg dispersed in 0.5 mL ethanol through sonication). Cyclic voltammetry (CV) and charging-discharging (GCD) analyses were carried out within the potential window of -0.2 to 6 V at different scan rates 5, 10, 25, 50, 75 and 100 mV/s respectively. The EIS spectroscopy was carried out in the frequency range 10^6 Hz to 1 Hz and the applied amplitude was 0.005 V versus open circuit potential.

Figure. 4 shows the cyclic voltammetry of as-synthesized Mn_2O_3 which were carried out with different scan rate 5, 10, 25, 50, 75 and 100 mV/s respectively. The cyclic voltammetry curve reveals that as the scan rate is increases the oxidative as well as reductive current is increases simultaneously. This increase in the enclosed surface area is due to the internal charge transfer resistance and diffusion control process. As can be seen among all can rate the highest output redox current as well as largest quasi-rectangular enclosed CV area. Changing the scan rate (5, 10, 25, 50, 75 and 100 mV/s) similar CV shape observed indicating excellent electrochemical performance, high reversibility and good rate capability of the electrode. Similarly, figure 4(b) also represents the cyclic voltammetry of Mn_2O_3 at temperature 700 ºC with the same scan rate as it has been done in 500 ºC. At 700 ºC also cyclic voltammetry shows that the graph is appeared as quasi-rectangular shape with the high degree of reversibility. But from graph it has been observed that the redox current as well as the enclosed surface area is decreasing with the increases in temperature.

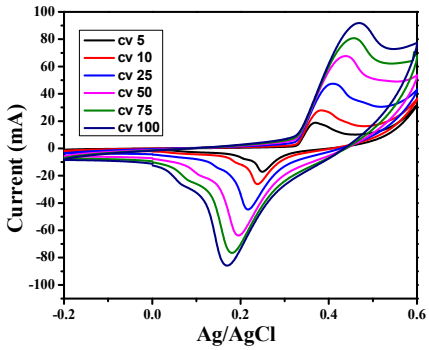

Figure.4 (a) Cyclic voltammetry of Mn_2O_3 at 500 ºC with different scan rate.

For quantitative measurement, Specific capacitance, energy density and power density of all prepared samples were calculated using the following formulae:

Specific Capacitance (F/g) = $\int$ IdV / m x SR x V ..... (2)

Energy Density (Wh/kg) = ½ CV^2 ..... (3)

Power Density (W/kg) = E/Δt .....(4)

Where, I = Current, m = Active mass, V = Potential, SR = Scan Rate (mV/s),
C = Specific Capacitance, Δt = Time (sec),
E = Energy Density

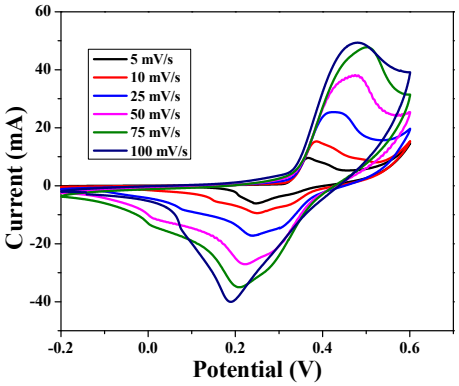

Figure.4 (b) Cyclic voltammetry of Mn_2O_3 at 700 ºC with different scan rate.

Table-1
Detail Electrochemical measurement of Mn_2O_3 at 500^{0}C

Mass loading	Scan rate	Area	Specific capacitance	Energy density	Power density
0.036	5	10.8	75.28	5.12	51.23
0.036	10	14.4	49.99	4.44	88.87
0.036	25	22.1	30.70	2.72	136.46
0.036	50	33.6	23.35	2.07	207.58
0.036	75	45.8	21.21	1.82	282.80
0.036	100	57.7	20.02	1.77	355.97

Table-2
Detail Electrochemical measurement of Mn_2O_3 at 700!

Mass Loading	Scan rate	Area	Specific capacitance	Energy density	Power density
0.015	5	2.12	35.28	3.13	31.35
0.015	10	5.90	49.13	4.36	87.34
0.015	25	10.72	35.75	3.17	158.87
0.015	50	16.86	28.11	2.49	249.82
0.015	75	21.39	23.77	2.11	316.93
0.015	100	21.90	18.25	1.62	324.42

Figure.4 (b) Cyclic voltammetry of Mn_2O_3 at 700ºC with different scan rate.

The specific capacitance for Mn_2O_3 was calculated by using equation 2 as mentioned above. The specific capacitance at 500 ºC and 700 ºC was found 75.28 F/g and 35.26 F/g respectively at the lower scan rate of 5 mV/s. The detailed comparative study of calculated specific capacitance value with different scan rate is listed in table-1and 2 with two temperature 500 ºC and 700 ºC respectively.

From the above table it has been found that the specific capacitance value for the 500 ºC has higher than that of the 700 ºC. This decrease in the specific capacitance and the enclosed surface area is due to the high degree of agglomeration and bigger particles size as observed in the XRD analysis and also due to the uneven distribution of particle as seen in the SEM analysis. The energy and power density of the prepared sample also showing the same trend.

To further establish the material to be used as an electrode material for supercapacitor application we have studied the charging-discharging pattern for the material as shown in figure -5 (a and b). It has been observed that materials show deviation from linearity when studied at current density of 1 A/g indicating pseudocapacitive nature. As per the trend observed the higher discharge time for 500 ºC can be due to pseudo-capacitance contribution metal oxides. It means that the sample which has been calcined at 500 ºC has better electrochemical properties than that of the 700 ºC. This increase in the charge-discharge time could be attributed due to the two reasons. (i) Smaller particle size distribution, and (ii) due to uniform size distribution with some porous structure respectively. Charging-discharging analysis for consecutive 500 cycle (at a current density 1 Ag^{-1}) also revealed good electrochemical stability and cyclic stability with maximum specific capacitance retention of 78% at 500 ! and 73% at 700 ! respectively to the initial capacitance values as shown in figure-5 (c).

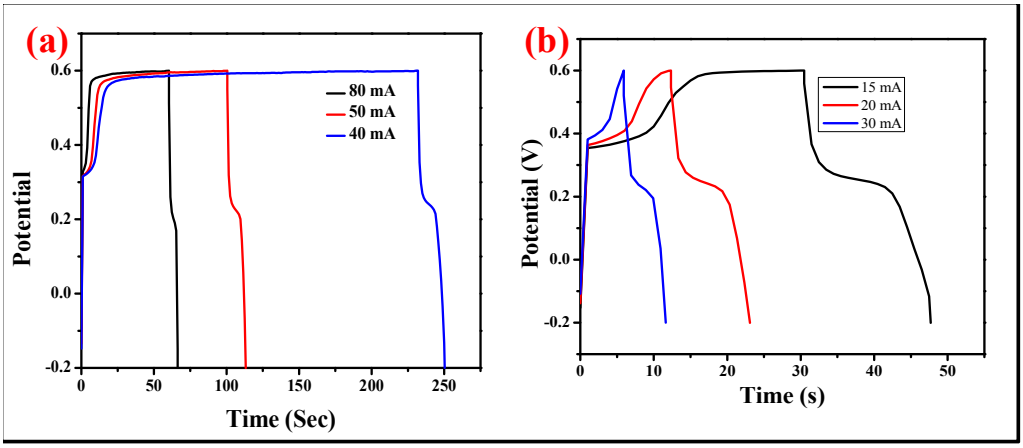

Figure. 5 (a and b) Galvanometric charge-discharge plots at temperature 500 ºC and 700 ºC.

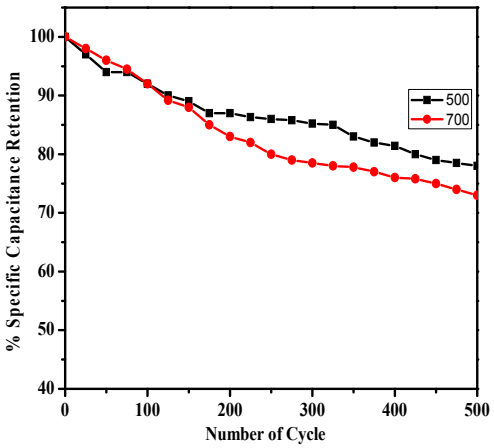

Figure. 5(c) Cyclic stability for consecutive 500 cycles.

Electrochemical impedance spectroscopy (EIS) analysis

The electrochemical impedance performance of prepared samples Mn_2O_3 was further confirmed by the Nyquist plot as presented in Figure 6. Nyquist plot is the plot between imaginary part (-Z") vs real part (Z') gives the frequency response of electrode-electrolyte system signifying about equivalent series resistance (ESR). X-intercepts of the real part gives the solution resistance (Rs) of material. The appearance of depressed semi-circle arc at high-frequency region indicates charge transfer resistance (Rct) attributed due to the porosity of the electrode material. The linear graph

obtained in the low-frequency region was due to the mass transfer phenomena during the electrochemical process. The straight line in the low-frequency region of EIS plot signifies the diffusion of the electrolyte within the electrode material. The sample having large semi-circle arc corresponds to the larger charge transfer resistance (Rct) value. It is noted from the graph that the charge transfer resistance of Mn_2O_3 at 500ºC has smaller than that of the Mn_2O_3 nanoparticles at 700ºC nanoparticles, which could be attributed due to the uniform particle size and uniform distribution of particle as observed in the SEM image. This decrease in the semi-circle arc at 500ºC is also showing that the material at this temperature has better conductive nature. Thus, it has been confirmed that the material (Mn_2O_3) at 500ºC is having better electrochemical behaviour than that of 700ºC.

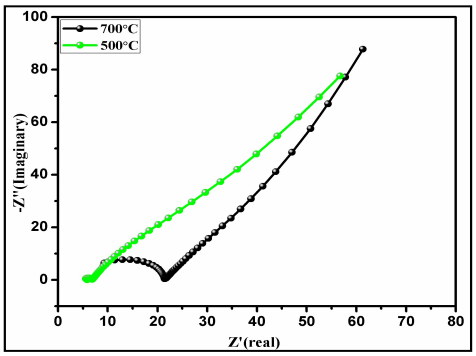

Figure-6 EIS analysis of prepared samples at temperatures 500 and 700!

Conclusion

In this study we have report a cost-effective sol-gel approach process for the synthesis Mn_2O_3 as electrode materials for supercapacitor application utilizing manganese nitrate ($Mn(NO_3)_2.4H_2O$) in 100 ml of ethylene glycol. The morphological analysis and successful formation of sample was confirmed by SEM, FTIR and XRD techniques. The materials at lower temperature reveals high surface area long with high-degree of porosity and active sites. The material had outstanding specific capacitance and capacitive behavior according to galvanostatic charge/discharge (GCD), cyclic voltammetry (CV), and complex impedance investigations. The synthesized Mn_2O_3 showed high specific capacitance (75.28 F/g and 35.28 F/g) at 5 mV/s at temperatures of 500 and 700 !. The materials high porosity improved the electrolyte-electrode contact and increased its specific area, making them suitable for energy storage.

Acknowledgements :

Authors would like to acknowledgement their institutions for providing infrastructures and financial support for this research work.

Conflict of interest :

Authors declare that they have no conflict of interest.

References

1. B. Raj, R. Oraon, M. Mohapatra, S. Basu, and A. K. Padhy, "Development of SnO_2@rGO Hybrid Nanocomposites through Complexometric Approach for Multi-Dimensional Electrochemical Application," *J. Electrochem. Soc.*, vol. 167, no. 16, p. 167518, (2020).
2. A. P. Dharani, G. Hariharan, M. Raja, P. Rajeshwaran, and S. Kumaran, "Improving the performance of Mn_2O_3 electrodes by Co substitution for super capacitor applications," *J. Mater. Sci. Mater. Electron.*, vol. 34, no. 28, p. 1959, 2023.
3. S. N. Amirtharaj and M. Mariappan, "Rapid and controllable synthesis of Mn2O3 nanorods via a

sonochemical method for supercapacitor electrode application," *Appl. Phys. A*, vol. 127, no. 8, p. 607, (2021).
4. M. R. Benzigar, V. D. B. C. Dasireddy, X. Guan, T. Wu, and G. Liu, "Advances on emerging materials for flexible supercapacitors: current trends and beyond," *Adv. Funct. Mater.*, vol. 30, no. 40, p. 2002993, (2020).
5. M. A. Hannan *et al.*, "Battery energy-storage system: A review of technologies, optimization objectives, constraints, approaches, and outstanding issues," *J. Energy Storage*, vol. 42, p. 103023, (2021).
6. J. Libich, J. Máca, J. Vondrák, O. ech, and M. SedlaYíková, "Supercapacitors: Properties and applications," *J. energy storage*, vol. 17, pp. 224–227, (2018).
7. S. Sharma, P. Chauhan, and S. Husain, "Structural and optical properties of Mn2O3 nanoparticles & its gas sensing applications," in *Adv. Mater. Proc.*, pp. 220 (2016)
8. W. Wei, X. Cui, W. Chen, and D. G. Ivey, "Manganese oxide-based materials as electrochemical supercapacitor electrodes," *Chem. Soc. Rev.*, vol. 40, no. 3, pp. 1697 (2011).
9. R. Ramkumar *et al.*, "MnO/Mn_2O_3 Aerogels as Effective Materials for Supercapacitor Applications," *Energies*, vol. 17, no. 10, p. 2258, (2024).
10. P. Mahajan, S. Verma, B. Padha, A. Ahmed, and S. Arya, "Manganese oxide and nickel oxide thin films on polyester to enable self-charging wearable supercapacitor," *J. Alloys Compd.*, vol. 968, p. 171904, (2023).
11. M. S. Waheed *et al.*, "Fabrication of mesoporous Er doped $ZnMnO_3$ nanoflake via sol gel approach for energy storage application," *Ceram. Int.*, vol. 49, no. 9, pp. 13298 (2023).
12. N. C. Horti *et al.*, "Optical and electrochemical properties of manganese oxide (Mn_3O_4) nanoparticles: Investigating the influence of calcination temperature on supercapacitor performance," *Mater. Chem. Phys.*, vol. 318, p. 129276 (2024).
13. Y. Kumar, S. Chopra, A. Gupta, Y. Kumar, S. J. Uke, and S. P. Mardikar, "Low temperature synthesis of MnO_2 nanostructures for supercapacitor application," *Mater. Sci. Energy Technol.*, vol. 3, pp. 566–574 (2020).
14. S.-I. Kim, J.-S. Lee, H.-J. Ahn, H.-K. Song, and J.-H. Jang, "Facile route to an efficient NiO supercapacitor with a three-dimensional nanonetwork morphology," *ACS Appl. Mater. Interfaces*, vol. 5, no. 5, pp. 1596 (2013).

An International Peer Reviewed Research Journal of Chemistry
Abstracted / Indexed in : Chemical Abstract U.S.A.
JC- 1607/2K25 (ISSN:0973-239X), INDIA
Journal Chemtracks Vol. 27 (1&2),9-18, January to December 2025